IET Energy Systems Integration

Special issue Call for Papers

**Be Seen. Be Cited.
Submit your work to a new
IET special issue**

Connect with researchers and experts in your field and share knowledge.

Be part of the latest research trends, faster.

Read more

IET The Institution of Engineering and Technology

IET Energy Systems Integration

ORIGINAL RESEARCH

Effective one-dimensional dynamic modelling of latent heat thermal energy storage units for heating applications

Hector Bastida | Ivan De la Cruz-Loredo | Carlos E. Ugalde-Loo

School of Engineering, Cardiff University, Cardiff, UK

Correspondence

Hector Bastida.
Email: BastidaHernandezJH@cardiff.ac.uk; hectorbas@hotmail.com

Abstract

Effective use of the energy stored within thermal energy storage systems requires mathematical models that faithfully represent the dynamics of interest. Although three-dimensional or two-dimensional models may provide an accurate representation of the thermal store, these are computationally intensive and may not be suitable for control system design or to simulate complex networks. Following this line, a low-order one-dimensional model of a latent heat thermal store is presented. The model is based on energy balance, the specific heat–temperature curve of the storage medium, and the dynamic calculation of the heat transfer coefficient. The simplicity afforded by the model facilitates its implementation in any programming language, guaranteeing its compatibility with commercial software to simulate complex systems. The model was implemented in MATLAB/Simulink and verified against experimental data of the real unit and simulation results obtained with a two-dimensional model. Simulation results for charging and discharging operations obtained with the one-dimensional model exhibit a root mean square error of ≤0.53 °C and a mean square error of ≤0.32 °C when compared with experimental results of the output temperature of the heat transfer fluid. These outcomes are deemed acceptable considering the low order of the one-dimensional model.

KEYWORDS

heating, latent heat, one-dimensional dynamic model, phase change material, reduced model, thermal energy storage

1 | INTRODUCTION

Energy storage units are often incorporated into energy systems to ensure demand is met under variable operating conditions and reduce operational costs. For instance, electrical batteries may help accommodate intermittent generation from renewable energy technologies such as photovoltaic panels or wind turbines to supply loads in electrical grids. For thermal systems, thermal energy storage (TES) units are essential components to improve the energy management. They facilitate the flexible management of thermal demand while considering the variability of gas and electricity tariffs when supplying heating or cooling through the use of gas boilers, combined heat and power (CHP) units or electric chillers [1, 2]. From the available TES technologies, latent heat TES (LHTES) and sensible heat

TES (SHTES) units have been successfully implemented in thermal systems to supply heating [3, 4] and cooling loads [5].

The storage temperature is critical when selecting the right TES unit for a thermal system and may depend on the type of thermal source, thermal load and the location of the thermal store [6]. For example, water tanks in some district heating systems store heat at ~90 °C using the sensible heat of water, while for residential applications LHTES units may store heat at ~60 °C for hot water provision [7]. The main advantage of using LHTES devices over SHTES-based options is their higher energy density. In an LHTES unit, a phase change material (PCM) is employed as the storage medium. A heat transfer fluid (HTF) is used to inject heat or take it out from the thermal store. The volume required by an LHTES unit to provide the same amount of energy as a SHTES unit is significantly smaller [8].

A change of phase in a PCM occurs within a narrow range of temperatures [9, 10]. However, there is a very wide variety of PCM commercially available, and its adequate selection will depend on the operating temperatures of the system of interest. Operating temperatures may be higher than 100 °C, where water would not be amenable as a storage medium. For example, waste heat from CHP units may be stored at high temperatures in waste heat recovery systems, where the exhaust gas temperature may reach over 300 °C [11]. Interested readers may refer to ref. [12] for a detailed review on LHTES systems and application examples.

Steady-state modelling is a commonly used approach for assessing the operation of energy systems supported by latent heat thermal stores [13, 14]. For instance, steady-state models are often integrated into optimisation algorithms aiming to minimise the operational costs or reduce carbon emissions [15, 16]. Although the storage capacity of the units is considered in these models, the heat transfer between the PCM and HTF is neglected. Constant values of the heat transfer coefficients are assumed, leading to a mathematical formulation based on algebraic equations which are solved through iterative methods [17, 18]. Although the modelling approach is simple, system dynamics cannot be assessed—and the models are thus limited. On the other hand, three-dimensional (3D) models may very accurately describe the thermal behaviour of an LHTES unit [19, 20]. The modelling approach enables a comprehensive description of heat transfer, with partial differential equations (PDEs) being adopted to define the balance of energy, mass and momentum. Several nodes are generated through a 3D mesh (which considers the x, y and z directions) to represent the volume of the thermal store. Given that the PDEs are solved for each node, a large computational time is normally required for simulations [21, 22].

If variations in one direction of a 3D model are neglected, for example, in the z-direction, a two-dimensional (2D) model is obtained, which in this case would consider the x and y directions only. Despite such simplification and decreased computational accuracy, 2D dynamic models remain suitable for LHTES unit design—particularly when investigating fin shapes or internal structures. Compared to a 3D model, the time to solve the equations describing heat transfer in a 2D representation may substantially decrease as the need for very resource-intensive computational methodologies is avoided. Such efficacy is reported in ref. [23], where a 2D model of an LHTES unit described by a large number of ordinary differential equations (ODEs) is presented (210,300 in total). The model is employed to assess the optimal design of fin shape to enhance thermal conductivity during heat transfer. Another example of a 2D model representing an LHTES unit is presented in ref. [24]. The TES unit is modelled using 7066 nodes. In the system under study, PCM in liquid state is recirculated using an external pump to increase the overall heat transfer coefficient of the thermal store by enhancing the melting process of the PCM.

In general, 2D models may be employed to accurately simulate the thermal dynamics of the HTF and PCM within LHTES units [25]. For instance, the 2D dynamic model of an LHTES unit for heating applications is presented in ref. [26]. In this reference, a dynamic calculation of the overall heat transfer

coefficient is carried out. This considers the thermophysical properties of the PCM and HTF as a function of temperature. A probability density function (PDF) is employed to describe the specific heat of the PCM. The 2D model was verified against experimental data, with a good match with simulation results reported in the reference. Nevertheless, the accuracy and efficiency achieved require an extensive set of 450 ODEs, alongside the adoption of the SundialsTB MATLAB toolbox, the sparse reverse Cuthill–McKee ordering algorithm and solver CVODE.

Reducing the number of ODEs in 2D models has been sought to decrease their computational cost. However, this should be done with care. As reported in ref. [27], such a reduction in a 2D model may cause sharp oscillations during its solution. To alleviate this issue, the model can be converted to a 'quasi-2D model' by considering heat transfer in the axial direction only, thereby ignoring radial variations, leading to a reduced set of ODEs.

While special solvers and a large set of ODEs are suitable for certain applications, they become less practical when analysing complex energy systems. Hence, the development of simplified models of LHTES units, which consider variations through a single direction only (e.g. x-direction), or one-dimensional (1D) models is not only attractive but also essential for simulating complex thermal networks. In general, the number of equations required to define a 1D model is considerably smaller compared to a 2D model. Employing a reduced equation set to describe heat transfer offers significant benefits in terms of the coding time for model implementation and computation time required for conducting simulations [28]. These advantages make the 1D modelling approach an ideal option to simulate the interactions of thermal stores with other components of heating systems, such as thermal sources, thermal loads, heat exchangers and hydraulic networks.

The utility of 1D models is further underscored by their incorporation into commercial software engines commonly adopted for simulating and analysing the operation of energy systems, such as Apros, TRNSYS and Modelica. Notably, despite employing different solvers and offering differing levels of modelling complexity, these software platforms fundamentally rely on 1D formulations. An example of a complex thermal network from a public health facility which considers SHTES units, CHP units, gas boilers, heat loads and hydraulic networks is reported in ref. [29]. In this case study, simulations were conducted using Apros to demonstrate the provision of operational flexibility afforded by the thermal stores—which are represented by 1D models.

The literature offers numerous references reporting 1D models with different levels of accuracy. For example, the model of an LHTES unit presented in ref. [30] assumes a constant value of enthalpy during the PCM's phase transition. This assumption, however, compromises the model's accuracy when comparing simulation results with experimental data. A more accurate 1D model of a commercial latent heat thermal store for heating applications is presented in ref. [18], where specific heat–temperature curves are used to quantify the PCM's specific latent heat. In ref. [28] a model of a commercial ice tank is presented, where ice is harvested to store cooling energy. Experimental data was employed to verify the validity

of simulation results. A great degree of accuracy was afforded by modelling the PCM's specific latent heat curve (i.e. water) using a PDF.

In this paper, a low-order 1D model of a latent heat thermal store for a heating application is presented and its performance is verified. The thermal store has a shell and tube structure. The model is formulated by a system of ODEs in terms of energy balance and considers the internal arrangement of the unit. The model also accounts for the thermophysical properties of the PCM and HTF within the temperature range of operation. Heat transfer is modelled dynamically and PDFs are adopted to describe the specific heat curve of the storage medium. The model was built in MATLAB/Simulink. To provide confidence in its accuracy, simulation results for charging and discharging operations were compared against simulation results obtained with a 2D model and experimental data (which are both available in ref. [26]).

The novelty of the model arises from its simplicity to reproduce relevant dynamics of a thermal store. For instance, for a 1D model spatially discretised into five nodes and defined by 10 ODEs only, model accuracy is not significantly affected. However, the amount of equations is reduced by ~98% compared to that of the 450 ODEs used in ref. [26] for the 2D model of the same LHTES unit investigated in this paper. Moreover, the portability of the 1D model facilitates its implementation in any programming language with an engine solver of non-linear ODEs. This may include commercial software where, to the best of the authors' knowledge, accurate models of LHTES units are currently unavailable.

The following are the key contributions of the paper:

- A detailed modelling formulation reflecting the internal configuration of the latent heat thermal store and relevant thermophysical data is presented, which allows for the model to be adjusted to different thermal stores and storage media.
- An easier implementation is facilitated by significantly reducing the number of ODEs required to model the thermal store compared to a 2D model of the same LHTES unit.
- A portable pseudo-code of the mathematical model suitable for implementation in any software engine featuring an ODE solver is provided.
- The suitability of the PDFs being used to accurately represent the PCM's specific latent heat curve and their adaptability are demonstrated.
- The 1D model was verified against experimental results available in the literature to provide confidence in the modelling approach, with simulation results leading to small errors when compared to the experimental data.

2 | SYSTEM DESCRIPTION

The LHTES unit investigated in this paper was originally presented in ref. [26], which also reports a 2D mathematical representation of the thermal store. It has a shell and tube internal configuration, where the shell is filled with the PCM Rigid-exHD6070EA, manufactured by INEOS [31]. This PCM, which offers a storage capacity between 10 and 15 kWh, is a high-density polyethylene with a low thermal conductivity. Therefore, metal fins are included in the unit to increase the PCM's thermal conductivity and thus improve heat transfer. The HTF employed is Marlotherm SH, which is a synthetic organic fluid manufactured by Eastman [32]. This is a low-viscosity medium with a boiling point of 392 °C, enabling its use for closed and forced-circulation heat transfer systems with high temperatures. The HTF circulates within 72 tubes made of P235GH (a carbon alloy steel [33]) from the front to the rear ports. A simplified schematic of the LHTES unit is shown in Figure 1, with relevant parameters for a single tube being provided in Appendix A.

Experimental data for the LHTES unit are reported in ref. [26]. The instrumentation in the experimental facilities considers flow rate and temperature sensors. The volumetric flow rate of the HTF was measured using an ultrasonic flow metre (Flexim Umfluxus F6) [34]. Platinum thermometers were located at the inlet and outlet of the LHTES unit to measure the temperature of the HTF. For clarity, the measurements from these sensors are identified in this paper as $T_{f,\text{in,e}}$ (°C) and $T_{f,\text{o,e}}$ (°C), where 'f' stands for HTF, 'in' for input, 'o' for output, and 'e' for experimental data. The PCM's temperature was measured using four thermocouple sensors located throughout the unit's length (of 2.5 m). Their axial positions from the front to the rear of the unit are $x_1 = 0.1$ m, $x_2 = 0.87$ m, $x_3 = 1.64$ m and $x_4 = 2.4$ m. The corresponding measurements from these sensors are denoted as $T_{p,1,\text{e}}$ (°C), $T_{p,2,\text{e}}$ (°C), $T_{p,3,\text{e}}$ (°C) and $T_{p,4,\text{e}}$ (°C), where 'p' stands for PCM.

The thermal energy supplied (or absorbed) by the HTF melts (or solidifies) the PCM surrounding the tubes. For modelling purposes, the PCM's volume affected by heat transfer is limited by bounds defined for each tube (i.e. a control volume) —forming a mesh through the LHTES unit. This is schematically shown in Figure 2. The control volume forms a cylindrical shape described by the PCM's radius r_p (m). This volume includes the HTF and the tube which, in turn, has dimensions defined by its external and internal radii r_{ext} (m) and r_{int} (m).
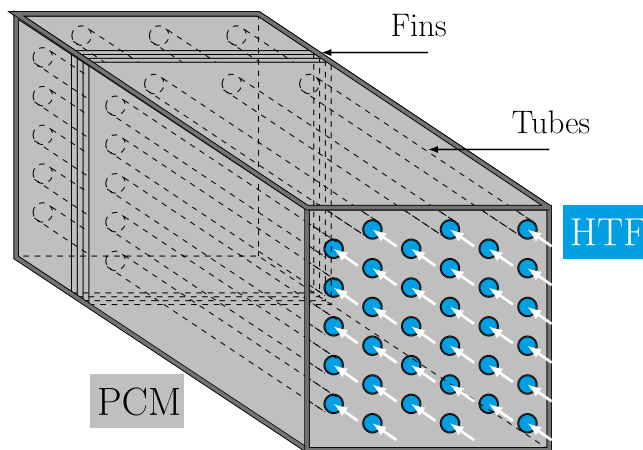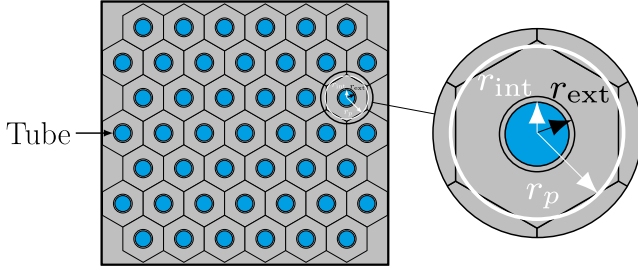

FIGURE 1 Schematic of the thermal store under investigation.

FIGURE 2 Cross-sectional view of the thermal store illustrating the cylindrical control volume.

This way, energy balance is used to describe the thermal dynamics within the thermal store.

3 | MODELLING APPROACH

The approach followed in ref. [28] to model an ice tank for cooling systems was adopted to develop the 1D mathematical representation of the thermal store shown in Figure 1. Heat transfer is described considering radial conduction between the tubes and the storage medium and forced convection between the HTF and the tube's internal wall. The density, thermal conductivity, and viscosity of the HTF, tube and PCM are considered in the model and their values presented in Appendix A. The specific heat curve of the PCM as a function of temperature is used to describe its phase change. A temperature range is established where the transition from solid to liquid occurs and vice versa. During this phase transition, specific latent heat is released or absorbed.

Three important assumptions have been made for the 1D model. Firstly, a well-insulated thermal store is assumed. Thus, thermal losses to the surrounding environment are neglected. Secondly, for all tubes, equal internal flow conditions and equal temperature distributions are considered. Therefore, describing the energy balance for one tube is sufficient to depict the thermal behaviour of all tubes. This enables spatially discretising the volume of a single tube to define the control volumes where energy balance is applied. Finally, the thermal dynamics of the LHTES unit are defined by a pair of ODEs for each control volume.

3.1 | Energy balance

Figure 3 shows a schematic for a single tube bounded by a control volume. This considers the volume of the HTF flowing within the tube, the tube's wall and the PCM around the tube, whose cylindrical shape is defined by r_p. Charging and discharging operations of the thermal store occur due to the energy transferred through the tube's wall between the PCM and HTF.

Heat transfer is described using the law of energy conservation with respect to the control volume. In general, the rate $\dot{E}_{st}$ (W) at which the internal energy of the thermal store changes is given by the following equation:
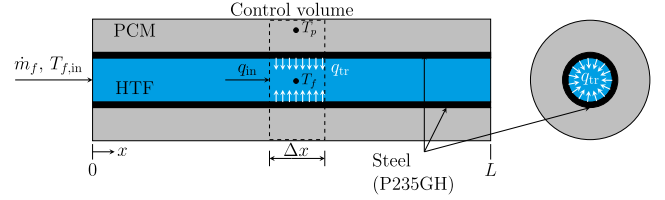
FIGURE 3 Schematic of a tube within the thermal store. The control volume is enclosed by the dashed black rectangle. The white arrows represent heat flowing towards the HTF.

$$\dot{E}_{st} = m_{st}c\dot{T}_{st} = \dot{Q}_{in} - \dot{Q}_{out}, \quad (1)$$

where m_{st} (kg) is the storage unit's mass and c (J/(kg°C)) the specific heat capacity of the storage medium at a temperature T_{st} (°C). This change in energy is given by the summation of heat flow rates entering and leaving the control volume $\dot{Q}_{in}$ (W) and $\dot{Q}_{out}$ (W). In turn, $\dot{Q}_{in}$ and $\dot{Q}_{out}$ result from a combination of heat transfer effects taking place in the system boundaries.

For the LHTES unit, the main heat contributions are split into the following equations:

$$\dot{E}_f = m_f c_{p,f} \dot{T}_f = \dot{m}_f c_{p,f} \left(T_{f,in} - T_f\right) + UA_{tr}\left(T_p - T_f\right), \quad (2)$$

$$\dot{E}_p = m_p c_{p,p} \dot{T}_p = UA_{tr}\left(T_f - T_p\right), \quad (3)$$

where $\dot{E}_f$ and $\dot{E}_p$ (W) are the rates of change in the internal energy of the HTF and PCM, m_f and m_p (kg) are the masses of the HTF and the PCM's control volume, $T_{f,in}$ (°C) is the inflow temperature, T_f and T_p (°C) are the temperatures of the HTF and PCM, respectively, and U (W/(m²°C)) and A_{tr} (m²) are the overall heat transfer coefficient and the heat transfer area, respectively, between the PCM and the HTF. Given that the HTF circulates through the latent heat storage system, a term for the energy advection is included in (2), where $\dot{m}_f$ (kg/s) is the mass flow rate of the HTF passing through and $c_{p,f}$ (J/(kg°C)) is its sensible specific heat capacity. In (3), $c_{p,p}$ (J/(kg°C)) is the specific heat of the PCM, which is a function of temperature.

U in (2) and (3) is a non-linear parameter, which is calculated from the flow and temperature conditions and the tube's conductivity where the HTF flows. The procedure to calculate U is described in detail in ref. [28].

3.2 | Spatial discretisation of the model

Spatial discretisation is necessary to accurately capture the thermal dynamics of the LHTES unit due to temperature changes in the HTF and PCM. This approach has been followed in the modelling of heat exchangers [35, 36], hydraulic networks [37] and SHTES units [38]. A tube carrying an HTF is considered to illustrate this process. The tube is divided into several discrete nodes as shown in Figure 4. Thus, the energy balance described in Section 3.1 is defined for each node

within the control volume. As previously discussed, since equal thermal and hydraulic conditions for all tubes are considered, the LHTES unit is analysed using a single tube instead of the 72 tubes in the tank. This assumption significantly reduces the number of equations required for the 1D model.

Spatial discretisation leads to a system of non-linear ODEs describing the temperature of the HTF and PCM. Since each node considers two equations, the order of the model is thus $2N$, where N denotes the number of nodes. In matrix form, this is described as the following equation:

$$
\begin{bmatrix}
\dot{T}_{f,1} \\
\dot{T}_{p,1} \\
\vdots \\
\dot{T}_{f,i} \\
\dot{T}_{p,i} \\
\vdots \\
\dot{T}_{f,N} \\
\dot{T}_{p,N}
\end{bmatrix}
=
\begin{bmatrix}
\dfrac{\dot{m}_f c_{pf,1}\left(T_{f,\mathrm{in}}-T_{f,1}\right)+U(A_{\mathrm{tr}}/N)\left(T_{p,1}-T_{f,1}\right)}{\rho_{f,1}c_{pf,1}\left(V_f/N\right)} \\[2ex]
\dfrac{U(A_{\mathrm{tr}}/N)\left(T_{f,1}-T_{p,1}\right)}{\rho_{p,1}c_{p,p,1}\left(V_p/N\right)} \\[2ex]
\vdots \\[1ex]
\dfrac{\dot{m}_f c_{pf,i}\left(T_{f,i-1}-T_{f,i}\right)+U(A_{\mathrm{tr}}/N)\left(T_{p,i}-T_{f,i}\right)}{\rho_{f,i}c_{pf,i}\left(V_f/N\right)} \\[2ex]
\dfrac{U(A_{\mathrm{tr}}/N)\left(T_{f,i}-T_{p,i}\right)}{\rho_{p,i}c_{p,p,i}\left(V_p/N\right)} \\[2ex]
\vdots \\[1ex]
\dfrac{\dot{m}_f c_{pf,N-1}\left(T_{f,N-1}-T_N\right)+U(A_{\mathrm{tr}}/N)\left(T_{p,N}-T_{f,N}\right)}{\rho_{f,N}c_{pf,N}\left(V_f/N\right)} \\[2ex]
\dfrac{U(A_{\mathrm{tr}}/N)\left(T_{f,N}-T_{p,N}\right)}{\rho_{p,N}c_{p,p,N}\left(V_p/N\right)}
\end{bmatrix}.
\tag{4}
$$

3.3 | Specific heat–temperature curve

Although an accurate representation of the phase transition of a PCM requires knowledge of its liquid fraction, this can also be modelled using specific heat curves as a function of temperature. In general, the availability of these curves facilitates the implementation of 1D and 2D models. They are essential to define the energy balance in (3) for the 1D model presented in this paper.
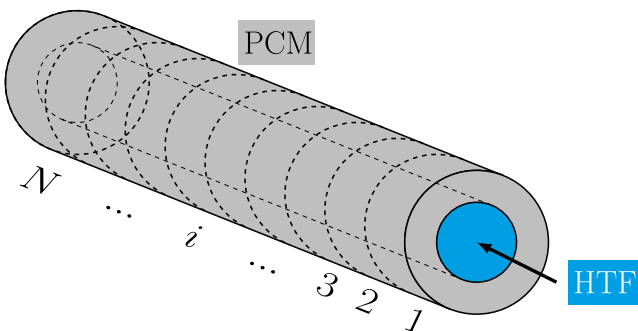

FIGURE 4 Single tube discretised into N nodes.

Specific heat–temperature curves may be experimentally determined with differential scanning or three-layer calorimetry methods [39, 40] and are usually provided by manufacturers alongside other properties of the PCM. In turn, they may be mathematically expressed using a PDF. This approach is discussed next.

Let the total storage capacity E_{tot} (J) of an LHTES unit be denoted by the following equation [28]:

$$
E_{\mathrm{tot}} = \Delta h_l m_{p,\mathrm{tot}},
\tag{5}
$$

where $m_{p,\mathrm{tot}}$ (kg) is the PCM's total mass and Δh_l (J/kg) is the specific latent heat value (i.e. the total amount of heat absorbed or released when the PCM changes phase per unit of mass [41]). Such a change in the internal thermal energy occurs within a well-defined temperature range, where the maximum energy released or absorbed occurs at a peak temperature. This process is quantified using the specific enthalpy–temperature curve, which is, in turn, defined using the relationship between the specific enthalpy h_p (kg/s) and the specific heat $c_{p,p}$ (J/(kg°C)) of the PCM as given below:

$$
h_p(T) = \int c_{p,p}(T_p)\, dT_p.
\tag{6}
$$

Thus, if the temperature range defined by the limits T_1 (°C) and T_2 (°C) where the phase change occurs is known, the specific latent heat is calculated with the following equation:

$$
\Delta h_l = \int_{T_1}^{T_2} c_{p,p}(T_p)\, dT_p.
\tag{7}
$$

The PCM's specific heat curve as a function of temperature T_p is obtained by differentiating (6). Mathematically, this is expressed using a PDF as given by the following equation:

$$
c_{p,p}(T_p) = a_0 + a_1 T_p + b_1 \varphi(T_p),
\tag{8}
$$

where a_0, a_1, and b_1 are dimensionless coefficients and φ represents the PDF.

In ref. [26], different PDFs were used to define specific heat curves. The Weibull minimum distribution is described by the following equation:

$$
\varphi^{\mathrm{W}} =
\begin{cases}
\dfrac{\gamma}{\theta}\left(-\dfrac{T_p-\eta}{\theta}\right)^{\gamma-1}\exp\left[\left(\dfrac{T_p-\eta}{\theta}\right)^{\gamma}\right] & T_p < \eta \\[3ex]
0, & T_p \ge \eta
\end{cases},
\tag{9}
$$

An adaptation of the Lognormal distribution is given as the following equation:

$$
\varphi^{\mathrm{L}} =
\begin{cases}
\dfrac{\exp\left[-\left((\ln[-(T_p-\eta)/\theta])^2/(2\gamma^2)\right)\right]}{-(T_p-\eta)\gamma\sqrt{2\pi}}, & T < \eta \\[3ex]
0, & T_p \ge \eta
\end{cases},
\tag{10}
$$

An adaptation of the Gumbel distribution is given as the following equation:

$$\varphi^{\mathrm{G}} = \left(\frac{1}{\theta}\right) \exp\left(\frac{T_p - \eta}{\theta}\right) \exp\left[-\exp\left(\frac{T_p - \eta}{\theta}\right)\right]. \quad (11)$$

In (9)–(11), η, θ, and γ are called the location, scale and shape parameters (all dimensionless), respectively. By suitably modifying the values of η, θ, and γ, accurate specific heat–temperature curves can be characterised such as those provided by PCM manufacturers. For instance, these parameters were estimated in ref. [26] to ensure a good match between experimental data and simulation results obtained with the 2D model of the same LHTES unit investigated in this paper. Such an approach was followed in ref. [28], where the dimensionless parameters of a Lognormal PDF for an ice TES tank were obtained heuristically.

Figure 5 shows the specific heat–temperature curves derived in ref. [26] alongside their corresponding specific enthalpy–temperature curves. Using these curves, the amount of thermal energy released (or absorbed) during the PCM's phase transition is calculated simply by knowing its temperature. The parameters of each PDF and the corresponding coefficients of (8) are shown in Table 1.

The PCM used in the LHTES unit investigated in this paper exhibits enthalpy hysteresis. Thus, since the melting temperature and the amount of latent heat for charging and discharging are different, separate curves for each process may be employed to accurately model the thermal behaviour of the thermal store. The Weibull minimum distribution is used to characterise the charging process, while the Lognormal distribution is used for discharging. However, a single specific heat–temperature curve may be adopted to facilitate the implementation of the thermal store model and, in turn, to easily enable simulations which consider cyclic charging and discharging processes. To this end, the Gumbel distribution is used, which has a melting temperature at ~125 °C (which lies between the melting temperatures of the Weibull and Lognormal distributions). To ensure the correct quantification of the specific latent heat stored and released by the thermal store, the left ends of the Gumbel and Lognormal PDFs at ~110 °C and the right ends of the Gumbel and Weibull PDFs at ~140 °C coincide, as shown in Figure 5a. This can also be noticed in Figure 5b, where the release and absorption of the specific latent heat are shown through a change in the slope of the specific enthalpy–temperature curves.

3.4 | On the similarities and differences of the model compared to other relevant 1D representations

The modelling approach presented in this section follows the same physics principles as in ref. [28]—and more specifically the law of conservation of energy. Both mathematical formulations are based on the definition of control volumes where energy balance is applied. Both models also adopt a 1D spatial discretisation method for the control volumes (akin to thermal stratification). However, the models exhibit two significant differences. Firstly, the model in ref. [28] was developed for an
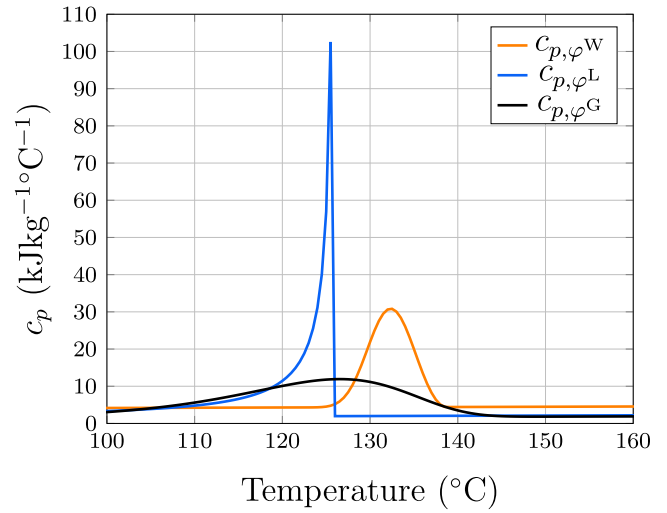
(a)
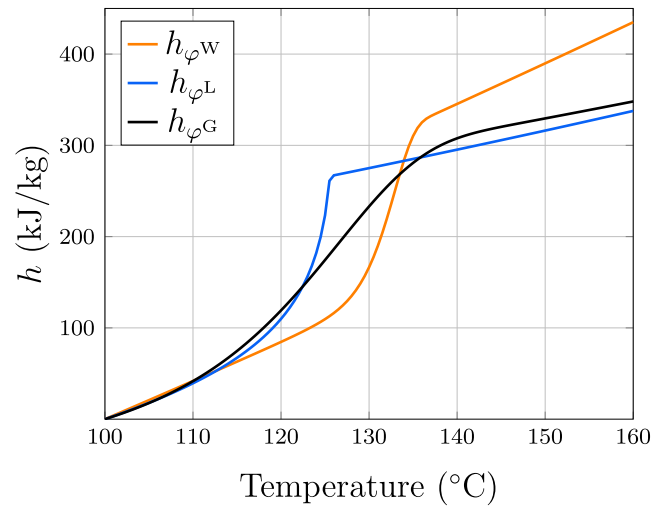
(b)

FIGURE 5 (a) Specific heat–temperature curves used in [26] to run simulations of charging and discharging processes. (b) Enthalpy curves. Subscripts 'φ^{W}', 'φ^{L}' and 'φ^{G}' refer to the Weibull, Lognormal, and Gumbel PDFs.

TABLE 1 Dimensionless coefficients in [26] to characterise specific heat–temperature curves.

	a_0	a_1	b_1	Parameters of φ
$c_{p,\varphi^{\mathrm{W}}}$	3501.6	6.5655	167.17×10^3	$\eta = 138.7, \gamma = 2.94, \theta = 7.33$
$c_{p,\varphi^{\mathrm{L}}}$	1137.2	6.5655	283.56×10^3	$\eta = 125.6, \gamma = 2.12, \theta = 4.80$
$c_{p,\varphi^{\mathrm{G}}}$	840.5	6.5655	261.55×10^3	$\eta = 126.5, \theta = 9.34$

ice tank used in cooling applications. This LHTES unit uses water as PCM and a mixture of water-glycol at 34% as HTF. In contrast, the model presented in this section was developed for an LHTES unit utilised in heating applications. This thermal store uses the high-density polyethylene RigidexHD6070EA as PCM and the synthetic organic fluid Marlotherm SH as HTF.

The HTF and PCM in this paper present different thermo-physical properties, specific heat curves as a function of temperature, and in the case of the PCM, different melting temperatures when compared to water and water-glycol in an ice tank.

The second important difference between the 1D model introduced in ref. [28] and the one in this paper is the internal structure of the thermal store. The LHTES unit presented here uses single straight horizontal tubes to circulate the HTF. In contrast, the ice tank modelled in ref. [28] uses an arrangement of spiral pairs of polyethylene tubes to circulate the HTF, which duplicates the number of equations required to model the LHTES unit. Due to the differences in the physical arrangements, types of HTF and PCM adopted, and, more importantly, in the thermal store application (heating vs. cooling), it is not possible to perform a direct comparison between the models to assess their performance.

Other relevant 1D models following a similar modelling approach based on energy balance have been presented in the literature. For instance, the performance of thermal stores and their interaction with other elements of the heat supply system of a civic building were evaluated in ref. [29] using 1D models

for heat transfer without incurring a phase change. A SHTES unit such as the one presented in ref. [29] is fundamentally different from the thermal store presented in this paper, which is a latent heat unit which uses PCM as the medium to store thermal energy. Here, heat transfer mainly involves a change of phase in the PCM since a large amount of energy is stored or released at a relatively constant temperature. A direct comparison between the SHTES unit presented in ref. [29] and the one introduced in this paper is, thus, not applicable as they are essentially different TES technologies.

4 | SIMULATION RESULTS

Figure 6 shows screenshots of the MATLAB/Simulink implementation of the 1D model presented in Section 3. This was facilitated with S-functions. The thermophysical properties of the HTF and PCM and their temperature dependence were incorporated to the model using a look-up table. These properties are provided in polynomial form in Appendix A.

A state-space notation was adopted to describe the mathematical model as pseudo-code as given below:

$$
\begin{bmatrix} \dot{T}_{f,1} \\ \dot{T}_{w,1} \\ \vdots \\ \dot{T}_{f,i} \\ \dot{T}_{w,i} \\ \vdots \\ \dot{T}_{f,N} \\ \dot{T}_{w,N} \end{bmatrix} = \begin{bmatrix} \dot{x}(1) \\ \dot{x}(2) \\ \vdots \\ \dot{x}(k) \\ \dot{x}(k+1) \\ \vdots \\ \dot{x}(2N-1) \\ \dot{x}(2N) \end{bmatrix} = \begin{bmatrix} \dfrac{\dot{m}_f c_p(x(1))\left[T_{f,\text{in}} - x(1)\right] + U(A_{\text{tr}}/N)\left[x(2) - x(1)\right]}{\rho_f(x(1))\, c_{pf}(x(1))\, (V_f/N)} \\[2ex] \dfrac{U(A_{\text{tr}}/N)\left[x(1) - x(2)\right]}{\rho_w(x(2))\, c_{p,p}(x(2))\, (V_p/N)} \\[1ex] \vdots \\[1ex] \dfrac{\dot{m}_f c_p(x(k))\left[x(k-2) - x(k)\right] + U(A_{\text{tr}}/N)\left[x(k+1) - x(k)\right]}{\rho_f(x(k))\, c_{pf}(x(k))\, (V_f/N)} \\[2ex] \dfrac{U(A_{\text{tr}}/N)\left[x(k) - x(k+1)\right]}{\rho_w(x(k+1))\, c_{p,p}(x(k+1))\, (V_p/N)} \\[1ex] \vdots \\[1ex] \dfrac{\dot{m}_f c_p(x(2N-1))\left[x(2N-3) - x(2N-1)\right] + U(A_{\text{tr}}/N)\left[x(2N) - x(2N-1)\right]}{\rho_f(x(2N-1))\, c_{pf}(x(2N-1))\, (V_f/N)} \\[2ex] \dfrac{U(A_{\text{tr}}/N)\left[x(2N-1) - x(2N)\right]}{\rho_w(x(2N))\, c_{p,p}(x(2N))\, (V_p/N)} \end{bmatrix} \quad (12)
$$

of the TES unit. However, despite the adoption of energy balance and thermal stratification for modelling (i.e. spatial discretisation of control volumes), the thermal store in this reference is a sensible heat unit (a hot water tank) which relies on the temperature difference of the storage medium (water)

In (12), variable T was replaced by x to denote the outputs of the pseudo-code, which are the variables being solved for. The input variables are the mass flow rate $\dot{m}_f$ and the input temperature $T_{f,\text{in}}$ of the HTF. $\dot{m}_f$ is included in all nodes of the HTF and $T_{f,\text{in}}$ appears only in the first node as it represents the
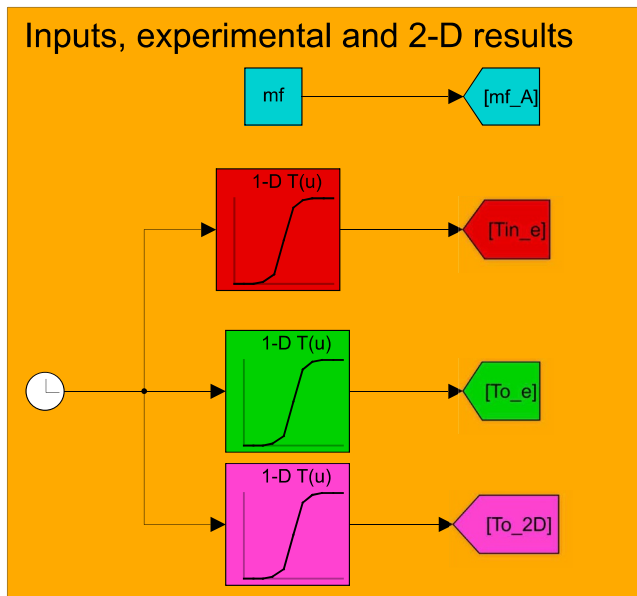
system's input temperature—and not the output temperature from the preceding node as it occurs for the remaining nodes. This was explicitly considered in the expression for the initial node. Input parameters include the thermophysical properties of the PCM and HTF, namely the temperature-dependent specific heat c_p, density ρ and the overall heat transfer coefficient U. System parameters include the heat transfer area A_{tr}, volume V and number of nodes N. The total number of equations is $2N$ as all control volumes are described by two equations.

This approach facilitates programming the equations using nested functions, which are in turn amenable to construct the S-functions in MATLAB/Simulink. Furthermore, this enables for an arbitrary selection of the number of nodes. However, as mentioned, the first node requires a separate definition as its input temperature corresponds to the overall system's input temperature.
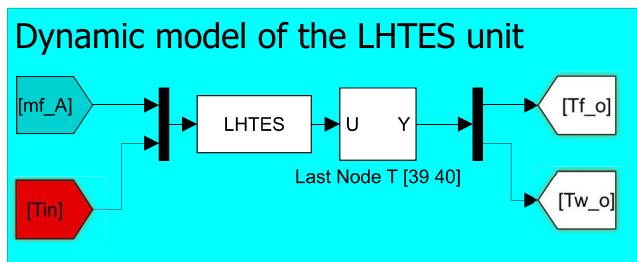
A comparison between simulation results of the thermal store obtained with the 1D model against simulation results using the 2D model reported in ref. [26] and experimental data included in the same reference are shown next. Experiments for both charging and discharging processes were conducted. A mass flow rate of $\dot{m}_f = 1.02$ kg/s was used for the HTF alongside different input temperature profiles ($T_{f,in,e}$). In the figure legends accompanying the results presented in the next sections, subscript 'e' denotes experimental data from ref. [26], 'f' stands for HTF, 'in' stands for input, 'o' stands for output, '2D' denotes simulation results from the 2D model in ref. [26] and '1D' denotes results from the 1D model presented in Section 3.

As suggested by ref. [28], a number of 20 nodes for spatial discretisation, and thus 40 ODEs, was initially selected for the 1D model as this was deemed sufficient for good accuracy. Such an accuracy may be, in turn, amenable to design control structures for the thermal store, such as state-of-charge (SoC) estimators [42]. To provide insight as to how the number of nodes affects model performance, a detailed analysis is presented in Section 5.
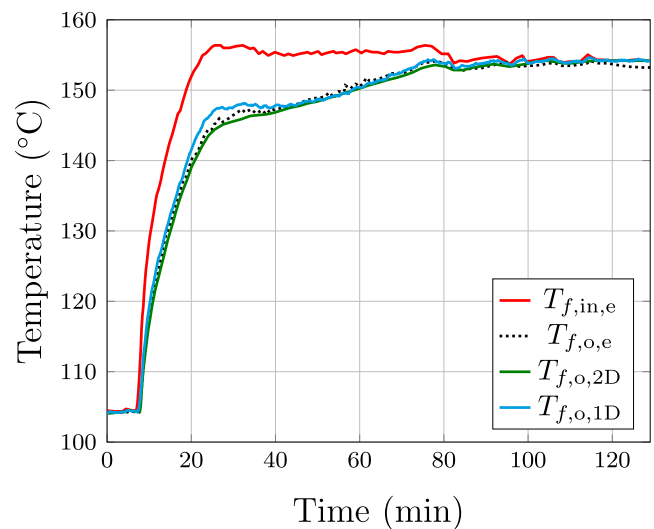
4.1 | Using different specific heat–temperature curves for charging and discharging

Figure 7 compares experimental data and simulation results for a charging process. The specific heat–temperature curve of the PCM employed in both the 1D and 2D models was characterised using the Weibull PDF illustrated in Figure 5a. Since the output of the HTF for the 1D model is the HTF's temperature in the last node (in this case node 20), then $T_{f,o,1D} = T_{f,20}$. The input profile $T_{f,in,e}$ (red trace) is included in the figure for reference. The simulation results obtained from both the 1D and 2D models ($T_{f,o,1D}$ in a light blue trace and $T_{f,o,2D}$ in a
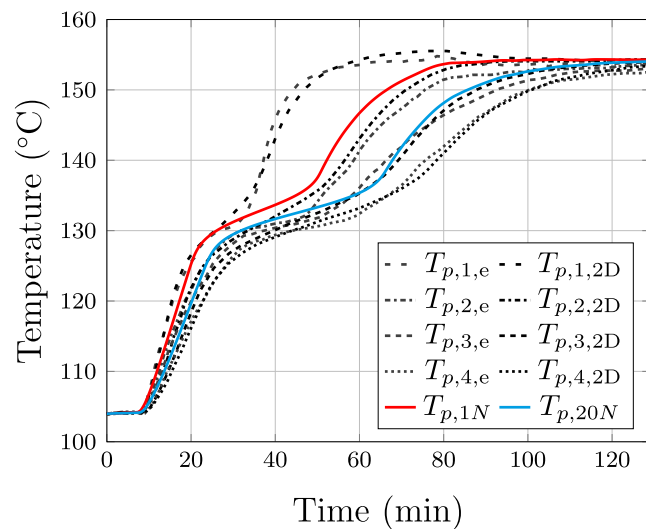
FIGURE 6 Model implementation in Simulink showing (a) system inputs, experimental data and results obtained from the 2D model and (b) S-functions representing the 1D model.

FIGURE 7 Comparison between experimental data $T_{f,o,e}$ (dotted black trace) and the simulation results of the 2D model ($T_{f,o,2D}$, green trace) and the 1D model ($T_{f,o,1D}$, light blue trace) for a charging process. The experimental temperature profile for the HTF is also shown ($T_{f,in,e}$, red trace).

green trace) agree with the experimental data ($T_{f,\mathrm{o,e}}$, dotted black trace). Thus, both models satisfactorily represent the output temperature of the HTF.

The temperature of the PCM monitored by the four sensors in the experimental unit (i.e. $T_{p,1,\mathrm{e}}$, $T_{p,2,\mathrm{e}}$, $T_{p,3,\mathrm{e}}$, $T_{p,4,\mathrm{e}}$) and selected simulation results obtained with the 1D and 2D models are shown in Figure 8. The experimental measurements are shown using a grey colour. The simulation results with the 2D model corresponding to each sensor measurement are shown with a black colour. Although in this case a direct comparison with the 1D model is not possible, the PCM temperatures in the first node ($T_{p,1N}$, red trace, located at x_{1N} = 0.0625 m) and last node ($T_{p,20N}$, cyan trace, x_{20N} = 2.435 m) are provided to facilitate the discussion.

Figure 8 reveals a divergence between the experimental data and results from simulations with the 1D model. In contrast, simulation results using the 2D model and the experimental data agree well. The discrepancy exhibited by the 1D model was expected as it considers the average temperature of a control volume only and, thus, the PCM node temperatures do not coincide with those obtained with its 2D counterpart. In contrast, the 2D model, which accounts for the axial and radial variation of temperature, exhibits a high accuracy. This is at the expense of requiring the definition of 450 nodes (and the same number of ODEs).

Figure 9 illustrates the temperature profiles of the PCM and HTF across all nodes throughout the charging process. This facilitates appreciating the PCM's melting process. The temperature shows a gradual variation across different node locations, with nodes located closer to the HTF inlet experiencing a more rapid increase in temperature compared to nodes near the HTF outlet. The heat being transferred between the PCM and HTF causes this difference, as the temperature of the HTF is higher early in the process at the beginning of the tube.
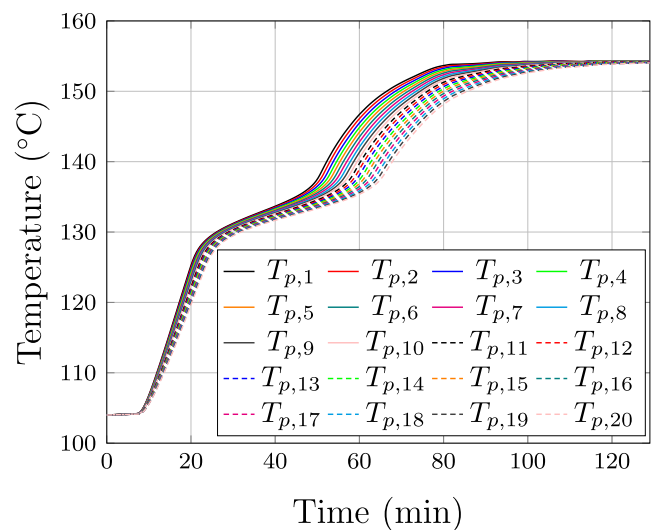
Figure 10 shows a comparison of experimental data and the simulation results for a discharging process. In this case, the PCM's specific heat–temperature curve was characterised with the Lognormal PDF shown in Figure 5a for both the 1D and 2D models. The input profile is also shown as a reference. It can be observed from these results that the 1D model is able to accurately capture the thermal dynamics of the HTF.

Figure 11 shows the behaviour of the PCM temperatures. As for charging, results from the 1D model for discharging deviate from the experimental data and the corresponding results from the 2D model. However, the characteristic 'shape' in the PCM temperature profiles exhibited by the experimental data is reproduced by the 1D model—even when the spatial discretisation limits its accuracy. This was also the case for the charging process (see Figure 8).
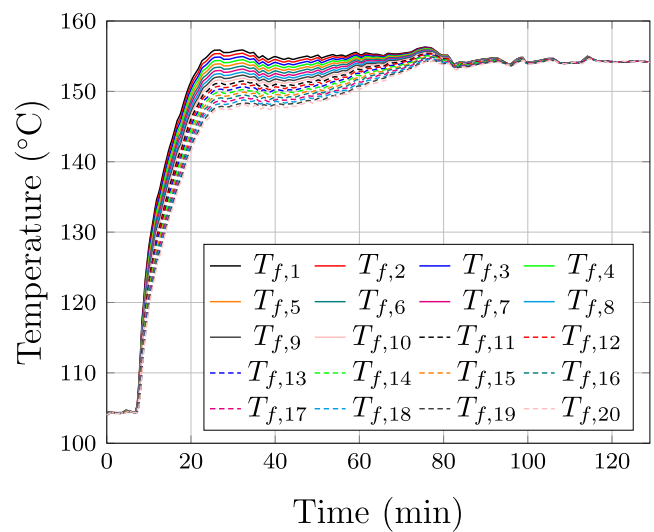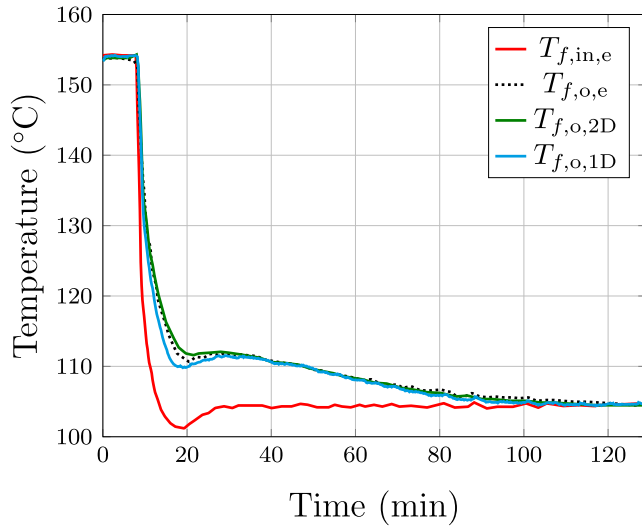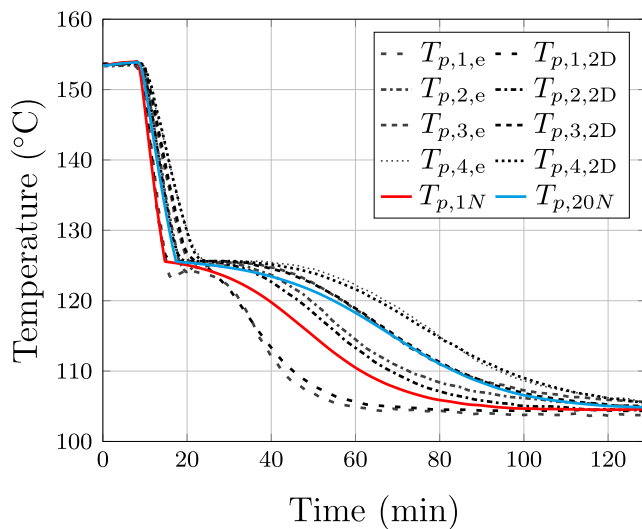

(a)

(b)

FIGURE 9 Node temperatures during charging process: (a) HTF; (b) PCM.

FIGURE 8 Comparison between the PCM temperatures monitored by four sensors ($T_{p,1,\mathrm{e}}$, $T_{p,2,\mathrm{e}}$, $T_{p,3,\mathrm{e}}$, $T_{p,4,\mathrm{e}}$) and the corresponding simulation results obtained with a 2D model ($T_{p,1,2D}$, $T_{p,2,2D}$, $T_{p,3,2D}$, $T_{p,4,2D}$) for a charging process. Results obtained with a 1D model for nodes 1 and 20 ($T_{p,1N}$ and $T_{p,20N}$) are included for discussion.

FIGURE 10 Comparison between experimental data $T_{f,o,e}$ (dotted black trace) and the simulation results of the 2D model ($T_{f,o,2D}$, green trace) and 1D model ($T_{f,o,1D}$, light blue trace) for discharging process. The experimental temperature profile for the HTF is also shown ($T_{f,in,e}$, red trace).

**FIGURE 11** Comparison between the PCM temperatures monitored by four sensors ($T_{p,1,e}$, $T_{p,2,e}$, $T_{p,3,e}$, $T_{p,4,e}$) and the corresponding simulation results obtained with a 2D model ($T_{p,1,2D}$, $T_{p,2,2D}$, $T_{p,3,2D}$, $T_{p,4,2D}$) for a discharging process. Results obtained with a 1D model for nodes 1 and 20 ($T_{p,1N}$ and $T_{p,20N}$) are included for discussion.

For completeness, the temperature gradient for all nodes of the 1D model is shown in Figure 12 during the discharging process to observe the solidification of the PCM. Similar to charging, the PCM solidification occurs faster for the nodes in close proximity to the HTF inlet. In contrast, the nodes closer to the HTF outlet exhibit a slower decrease in temperature.

Although the 1D model is not able to provide the accurate depiction of the temperature variations of the PCM afforded by the 2D model, this is not a shortcoming when assessing the operation of the thermal store within a thermal system. The
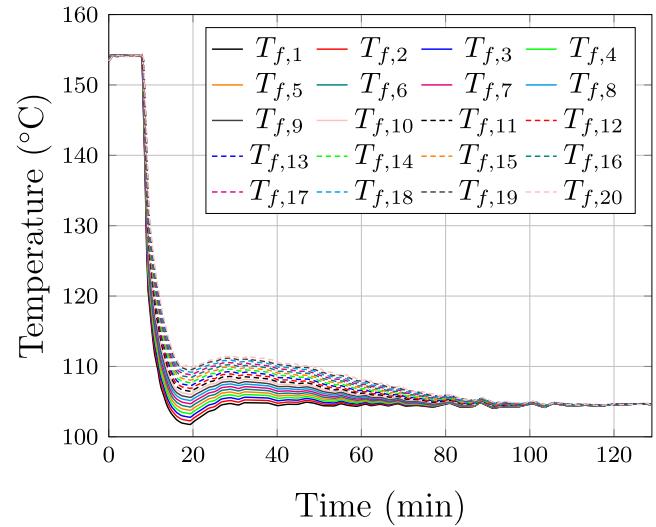
(a)
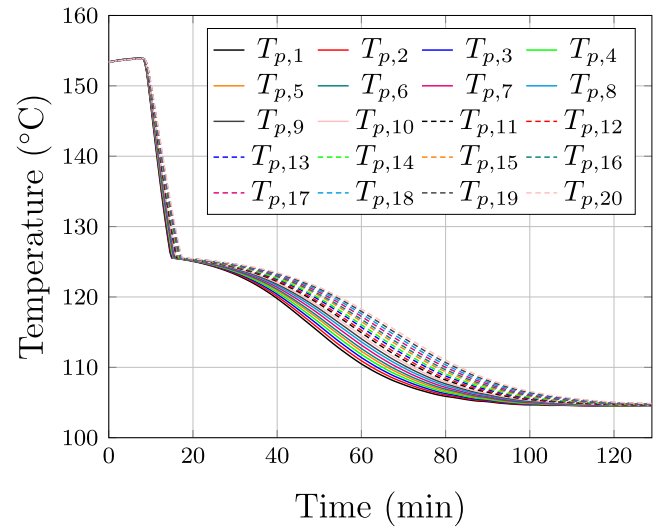
(b)

FIGURE 12 Node temperatures during discharging process: (a) HTF; (b) PCM.

key variable to monitor is the HTF's output temperature, as the energy stored by the PCM is transferred through the HTF. For system analysis, the model may be linked to other components, such as heat exchangers, which use the output temperature of the HTF as their input. Moreover, an accurate quantification of this temperature enables a reliable calculation of the energy provided by the LHTES unit. As shown in Figures 7 and 10, this is achieved with the 1D model.
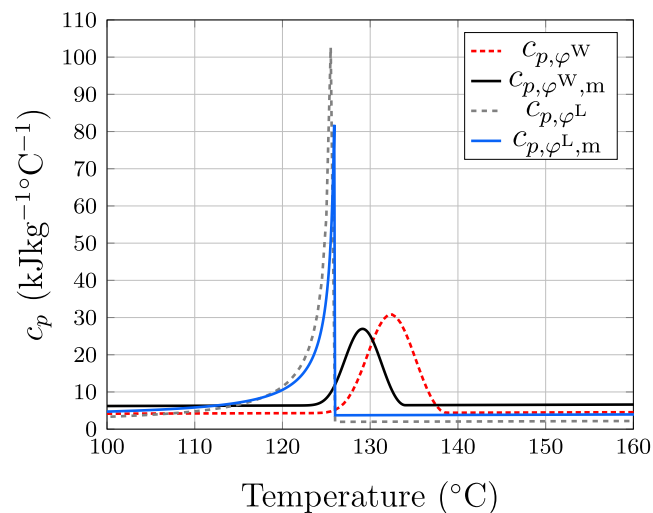
4.2 | Performance improvement of the 1D model and error analysis

The parameters of the PDFs representing the specific heat–temperature curves for charging and discharging were

heuristically adjusted in the 1D model to increase its accuracy, as these values had been specifically tuned in ref. [26] for a 2D model. Figure 13 shows a comparison between the specific heat–temperature curves adopted from ref. [26] and the new PDFs, where subscript 'm' is used to identify the modified curves. The parameters for the modified PDFs are shown in Table 2.

Figure 14 compares the experimental data (dotted black trace, $T_{f,o,e}$) and the simulation results using the 2D model (grey trace, $T_{f,o,2D}$) with the simulation results using the 1D model. The light blue trace shows the simulation results for the 1D model using the original PDFs ($T_{f,o,1D}$) and the green trace for when the modified PDFs are adopted ($T_{f,o,1D,m}$). The input profile (red trace, $T_{f,in,e}$) is shown for reference. The improved performance with the 1D model is evident in the charging process at ~20–40 min (see the zoomed-in window in Figure 14a), where $T_{f,o,1D,m}$ is closer to $T_{f,o,e}$ than $T_{f,o,1D}$. A similar improvement is notable for the discharging process between 10 and 25 min (see the zoomed-in window in Figure 14b).

To provide additional insight into the enhanced accuracy and reliability of the 1D model, an error analysis was carried out. This considers the calculation of the mean absolute error (MAE) and the root mean square error (RMSE) of the simulation results obtained with the different models measured against the experimental data. The results of the analysis are shown in Table 3, where the HTF's output temperature is the

variable used for the comparison. The 2D model exhibits smaller values of RMSE and MAE than the 1D model for both charging and discharging when the PDFs given in ref. [26] are

(a)
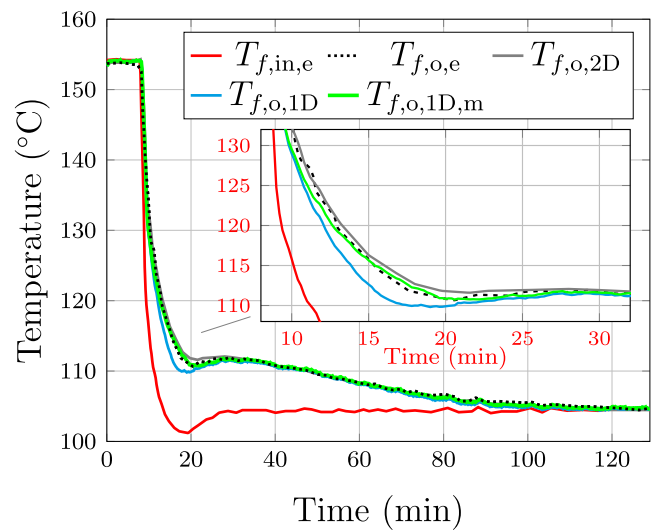
(b)

FIGURE 14 Simulation results of the charging and discharging processes employing modified PDFs.
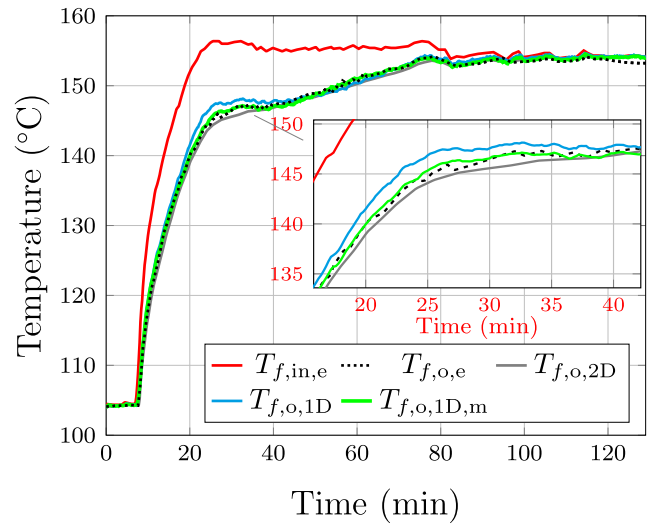

FIGURE 13 Comparison of original and modified Weibull and Lognormal PDFs.

TABLE 2 Parameters of the modified specific heat–temperature curves.

	a_0	a_1	b_1	Parameters of φ
c_{p,φ_m^W}	5556.2	6.5655	99.46×10^3	$\eta = 134, \gamma = 2.94, \theta = 5.62$
c_{p,φ_m^L}	2903.0	6.5655	220.07×10^3	$\eta = 126, \gamma = 2.12, \theta = 4.80$

TABLE 3 RMSE and MAE from simulation outputs obtained with the 2D and 1D models with respect to experimental measurements of the HTF output temperature.

Error	Charging		Discharging	
	RMSE	MAE	RMSE	MAE
$T_{f,o,2D}$ (°C)	0.61	0.51	0.48	0.31
$T_{f,o,1D}$ (°C)	0.81	0.62	0.93	0.58
$T_{f,o,1D,m}$ (°C)	0.39	0.30	0.52	0.28

Note: Different PDFs were employed for charging and discharging.

used for both models (see Table 1). Nevertheless, the errors for the 1D model significantly decrease when the modified PDFs are employed (see Table 2). For charging, both are reduced by more than half with the modified PDFs, and these values are even smaller for the 2D model. For discharging, although the RMSE and MAE do not reduce as dramatically when the modified PDFs are adopted, these are remarkably close to those obtained with the 2D model—with an absolute difference of less than 0.05 °C.

4.3 | Using a single specific heat–temperature curve for charging and discharging

An additional comparison of simulation results against experimental data was carried out. This considers eight distinct runs (four for charging and four for discharging) with different HTF's mass flow rates. A unique PDF was used for both the 1D and 2D models to characterise the PCM's specific heat–temperature curve. The rationale behind adopting a single PDF, in this case the Gumbel minimum distribution function in (11), was to employ a unique curve resembling the release and absorption of the specific latent heat for charging and discharging processes, as discussed in Section 3.3.

Figure 15 shows the comparison between the experimental data and the simulation results for all charging and discharging processes. The HTF's mass flow rate is provided in its corresponding graph. For reference, the HTF's input temperature profile is included (grey traces). As observed, the simulation results obtained with the 1D model (blue traces) are similar to those from the 2D model (red traces). However, both models exhibit a decrease in accuracy with respect to the experimental data (dotted black traces). This is confirmed by the error analysis summarised in Table 4, where the RMSE and MAE of the simulation results with relation to the experimental data are compared. As in Section 4.2, the HTF's output temperature was used for the analysis.

In general, both models exhibit larger errors when a single PDF is adopted for both charging and discharging (Table 2) compared to when two different PDFs are used (Table 4). This was expected, as using a PDF for charging and another one for discharging enables representing the PCM hysteresis more accurately. However, despite the decreased accuracy, using a unique specific heat curve as a function of temperature to characterise both charging and discharging simplifies the implementation of the thermal store models. This attribute is relevant, as the model will not need to anticipate whether a subsequent charging or discharging operation will take place given an arbitrary initial condition. Representing the right thermal dynamics will emerge naturally from the solutions of the ODEs—aided by the capabilities conferred by a unique PDF to characterise the specific heat behaviour as a function of temperature.

5 | ON THE ACCURACY AND COMPUTATION TIME OF THE 1D MODEL

5.1 | Effect of the number of nodes in the accuracy of the model

The results for the 1D model shown in Section 4 were obtained using a variable time step. The rationale behind this choice stemmed from the slow dynamics exhibited by the TES unit. For completeness, this section assesses the effect in accuracy of considering a different number of nodes for model discretisation.

A fixed time step of 0.5 s was adopted to achieve a good accuracy in the solutions of the ODEs representing the model. The 1D model was discretised into 5, 10, 20, 30, 50 and 100 nodes. Three simulations processes are analysed. Charging and discharging operations with the modified Weibull and Lognormal PDFs (see Table 2) are presented first. A simulation with cyclic charging and discharging processes is then discussed, for which the Gumbel PDF is used throughout (Table 1). Then, the stored energy and SoC were calculated and compared to values available in ref. [26].

Figure 16 shows the simulation results for the charging process using a 1D model with the modified Weibull PDF. A constant $\dot{m}_f = 1.02$ kg/s was used. The results obtained with the 2D model and experimental data are included for comparison. For clarity, only results with a variable time step are included. Subscript 'xN' within the figure legend corresponds to the total number of nodes for each discretised 1D model. The discrepancy between the HTF's output temperature when employing five nodes ($T_{f,5N}$, blue trace) compared to a model with 100 nodes ($T_{f,100N}$, magenta trace) is negligible. The zoomed-in window in the figure shows that this difference is about 0.1 °C. Regardless of the number of discretisation nodes employed, all 1D models offer a comparable performance.

To provide further insight, an error analysis was conducted as in previous sections of the paper. The RMSE and MAE were quantified against experimental data (using the HTF's output temperature) and compared with the errors exhibited by the 2D model. The comparison also considers when a fixed time step was used. The results are summarised in Table 5.

Notably, a model with 100 nodes (represented by 200 ODEs) brings very little reduction in the RMSE (of 0.04 °C) and MAE (of 0.03 °C) compared to when a model with five nodes, represented by 10 ODEs only, is adopted. This implies the accuracy of the model is not significantly improved as the number of nodes increases. Selecting a fixed time step brings virtually no difference in the model's accuracy compared to when a variable time step is adopted, with differences in RMSE and MAE being negligible. The errors exhibited by the 1D model are smaller, in all cases, than when the 2D model is employed—thus outperforming it.

Figure 17 shows the results for a discharging process of the 1D model with the modified Lognormal PDF. As in the
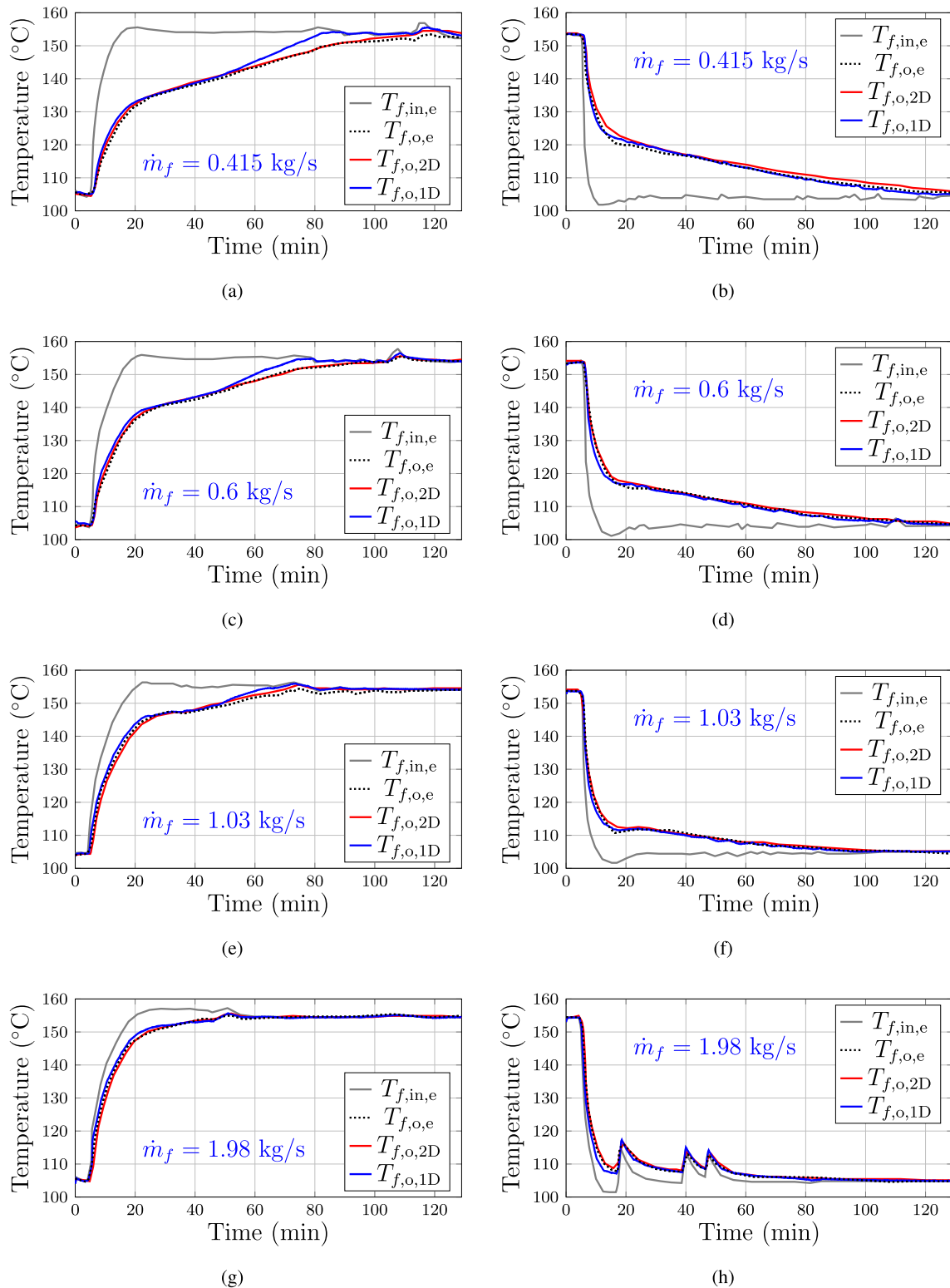
FIGURE 15 Simulations of the charging and discharging cycles at different $\dot{m}_f$. Experimental data of the HTF's output temperature ($T_{f,o,e}$) are compared against the simulation outputs derived from the 2D and 1D models ($T_{f,o,2D}$ and $T_{f,o,1D}$).

charging process, $\dot{m}_f = 1.02$ kg/s, and simulation outputs using the 2D model and experimental data were included for comparison. The 1D model exhibits a similar performance for all simulations regardless of the selected number of nodes. The zoomed-in window in the figure shows that the absolute

difference between the results using 1D models with 5 and 100 nodes is ~0.1 °C.

A detailed analysis of the RMSE and MAE was conducted, with results summarised in Table 5. In line with the results for the charging process, there is very limited improvement when

TABLE 4 RMSE and MAE from simulation results obtained with the 2D and 1D models with respect to experimental measurements of the HTF output temperature.

		Charging		Discharging	
		RMSE	MAE	RMSE	MAE
$\dot{m}_f$	$T_{f,o,2D}$ (°C)	0.85	0.69	1.32	1.11
0.495 kg/s	$T_{f,o,1D}$ (°C)	2.17	1.83	0.75	0.53
$\dot{m}_f$	$T_{f,o,2D}$ (°C)	0.52	0.40	0.58	0.44
0.6 kg/s	$T_{f,o,1D}$ (°C)	1.51	0.40	0.95	0.44
$\dot{m}_f$	$T_{f,o,2D}$ (°C)	0.99	0.87	0.61	0.44
1.03 kg/s	$T_{f,o,1D}$ (°C)	1.24	1.01	0.72	0.45
$\dot{m}_f$	$T_{f,o,2D}$ (°C)	0.74	0.44	0.58	0.43
1.98 kg/s	$T_{f,o,1D}$ (°C)	0.79	0.51	1.12	0.56

Note: A unique PDF was adopted for both charging and discharging.
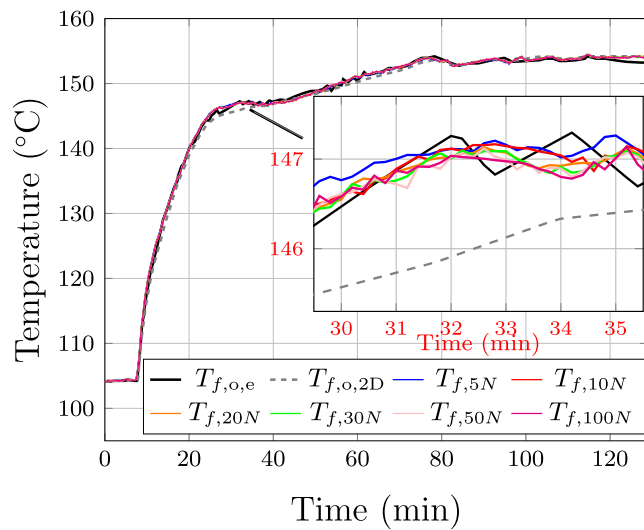
FIGURE 16 Comparison of the experimental data and simulation derived from the 2D model (HTF's output temperature) against simulation results of the 1D model for a charging process.

TABLE 5 RMSE and MAE from simulation results obtained with the 2D and 1D models ($T_{f,o,2D}$, T_{fxN}) with respect to experimental measurements of the HTF's output temperature.

	Charging		Discharging		Charging–discharging	
	RMSE	MAE	RMSE	MAE	RMSE	MAE
$T_{f,o,2D}$	0.61	0.51	0.48	0.31	1.41	0.92
$T_{f,5N}$ (Var)	0.42	0.32	0.53	0.28	2.25	1.92
$T_{f,5N}$ (Fix)	0.42	0.31	0.52	0.26	2.27	1.95
$T_{f,10N}$ (Var)	0.40	0.30	0.51	0.27	2.19	1.88
$T_{f,10N}$ (Fix)	0.39	0.30	0.50	0.26	2.18	1.86
$T_{f,20N}$ (Var)	0.40	0.30	0.52	0.28	2.14	1.82
$T_{f,20N}$ (Fix)	0.38	0.30	0.50	0.26	2.13	1.82
$T_{f,30N}$ (Var)	0.39	0.30	0.51	0.28	2.12	1.81
$T_{f,30N}$ (Fix)	0.38	0.29	0.50	0.26	2.11	1.80
$T_{f,50N}$ (Var)	0.38	0.29	0.51	0.28	2.11	1.80
$T_{f,50N}$ (Fix)	0.38	0.29	0.50	0.26	2.11	1.79
$T_{f,100N}$ (Var)	0.38	0.29	0.51	0.28	2.10	1.78
$T_{f,100N}$ (Fix)	0.38	0.29	0.51	0.26	2.10	1.79

Note: Errors were quantified for a charging process, for a discharging process, and for a simulation considering cyclic charging and discharging. In the rows, 'Var' stands for a variable time step and 'Fix' for a time step of 0.5 s for the setup of the engine solver in MATLAB/Simulink.

FIGURE 17 Comparison of the experimental data and simulation outputs derived from the 2D model (HTF's output temperature) against simulation results of the 1D model for a discharging process.
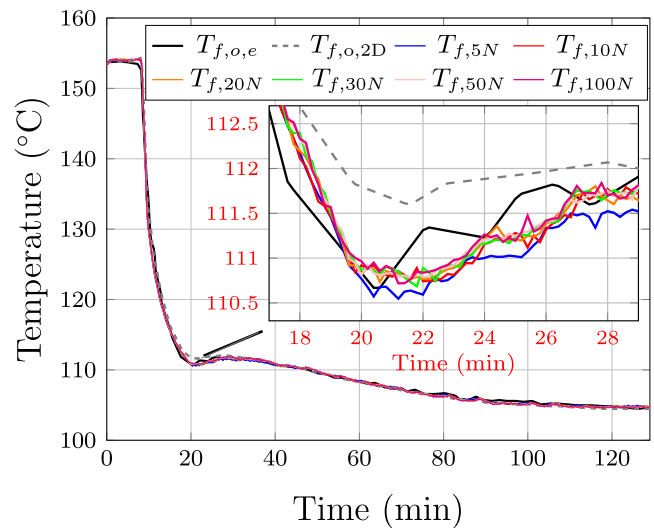
the number of nodes is increased from 5 to 100. When a variable step is used, the difference is 0.02 °C for the RMSE and no difference is evidenced for the MAE. For a fixed time step, these values are 0.01 and 0 °C. Neither increasing the number of nodes in the models nor adopting a small fixed time step for simulation leads to a substantial enhancement in accuracy. Notably, compared to the errors exhibited by the 2D model, the RMSE in all cases is similar and the MAE is always lower with the 1D model.

Figure 18 shows the simulation results for when a set of cyclic charging and discharging processes is conducted and the Gumbel PDF is adopted for both processes. A constant $\dot{m}_f = 1.09$ kg/s was maintained throughout. For completeness, results obtained with the 2D model and experimental data as presented in ref. [26] are shown. As in the previous simulations in this section, only results for the 1D model when a variable time step was used are shown for clarity. The

zoomed-in window in the figure shows a temperature difference between the model with 5 and 100 nodes of ~0.1 °C. The performance achieved with the 1D model with respect to the 2D model and experimental data is comparable.

To gain further insight into the results, an error analysis was conducted, with key metrics summarised in Table 5. Both the RMSE and MAE marginally decrease as the number of

nodes increases. However, these improvements are too small to be considered significant. This applies to both when a variable and a small fixed time step are used to conduct the simulations. Although the accuracy of the 1D model when five nodes are used is slightly lower than when a 2D model is adopted, this performance is considered acceptable (and a good compromise) given that the 1D model only requires 10 ODEs.
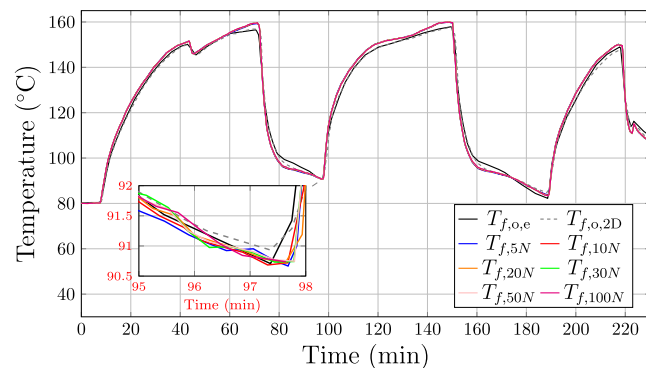
To provide additional insight into the performance of the presented 1D model, the stored energy E (kWh) and SoC (%) for the cyclic charging and discharging process shown in Figure 18 were compared with values obtained with the 2D model investigated in ref. [26].

For both the 1D and 2D models, E was determined by solving the following differential equation:

$$\frac{dE}{dt} = \dot{m}_f c_{pf} \left(T_{f,\text{in}}(t) - T_{f,o}(t) \right),\qquad(13)$$

which is a function of the difference between the input and output temperatures of the HTF, its mass flow rate and its specific heat–temperature curve.

Figure 19 compares the value of stored energy E obtained for the 1D and 2D models, with subscripts '1DX' and '2D' being adopted to denote each model and 'X' representing the number of nodes used in the simulation of 1D models. Results
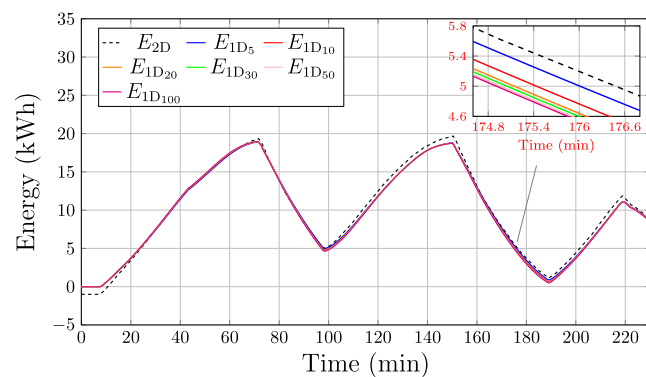
for six 1D representations with 5, 10, 20, 30, 50 and 100 nodes are shown (solid coloured traces) alongside the stored energy for the 2D model (black dotted trace). A negligible difference is observed among the 1D models regardless of the number of nodes being employed. Notably, the traces for the 1D model agree well with those of a more intricate 2D model.

To complement the previous observation, an error analysis was conducted, with key metrics summarised in Table 6. This considers calculation of the RMSE and MAE of E obtained with the 1D models when compared to the same variable obtained with the 2D model as provided in ref. [26]. As observed, the minimum error values, which are small, are exhibited by the 1D model with five nodes (RMSE of 0.47 kWh and MAE of 0.39 kWh). In addition, the absolute difference in these error metrics between a model with five nodes and one with 100 nodes is about 0.1 kWh for either error. These very slight differences confirm that regardless of the number of nodes employed in the 1D model, its accuracy is very similar to that provided by the 2D model.

For the 1D model, the SoC during the cyclic charging and discharging process shown in Figure 18 was determined using the method presented in ref. [42]. A description of the SoC calculation method is provided in Appendix B for completeness. In this approach, the specific latent heat Δh_l (J/kg) represents the portion of specific heat including the transition zone between liquid and solid phases—bounded by temperatures $T_{\text{empty}} = 109.5$ °C and $T_{\text{full}} = 138$ °C, which dictate whether the thermal store is fully charged or fully discharged. For the 2D model, SoC was derived from the specific heat–temperature curve of the PCM and the temperatures of all the 450 nodes, requiring to solve the mathematical model through integration in both axial and radial directions. The SoC data for the 2D model was borrowed from ref. [26].

Figure 20 shows the calculated SoC for 1D models with different number of nodes (5, 10, 20, 30, 50 and 100, solid coloured traces, SOC_X, where 'X' is the number of nodes) and the 2D model (black dotted trace, SOC_{2D}). The curve produced by the 2D model, which employs a substantially larger number of 450 nodes, slightly deviates from those traces obtained with the 1D models. This discrepancy results from the 2D model exhibiting a resolution of seven radial temperatures per PCM node compared to a single average temperature value

FIGURE 18 Comparison of the experimental data and simulation results of the 2D model (HTF's output temperature) against simulation results of the 1D model for cyclic charging and discharging processes.

FIGURE 19 Comparison of the total stored energy calculated with the 2D from ref. [26] and 1D models with different number of nodes.

TABLE 6 RMSE and MAE of the stored energy E and SoC obtained with 1D models with different number of nodes when compared to calculations with the 2D model.

| Nodes	Energy (kWh)		SoC (%)	
	RMSE	MAE	RMSE	MAE
5	0.47	0.39	5.45	4.27
10	0.51	0.42	5.73	4.39
20	0.54	0.45	5.9	4.47
30	0.55	0.46	5.97	4.5
40	0.56	0.47	6.01	4.53
50	0.57	0.48	6.05	4.55

per node afforded by a 1D model, which inevitably impacts SoC calculation. To provide further insight, as with the stored energy, the RMSEs and MAEs between the SoC for the 2D model and those obtained for the 1D models are also shown in Table 6. As it can be observed, even if a 1D model with only five nodes is adopted, the error metrics when compared to the 2D model are 5.45% for the RMSE and 4.27% for the MAE. This level of accuracy is notable, especially when considering that this 1D model was formulated with 10 ODEs only—in contrast to the 2D model requiring 450 ODEs.

5.2 | Effect of the number of nodes in the computation time

A key advantage of the 1D model presented in this paper lies in its simplicity to describe the thermal behaviour of an LHTES unit as it is characterised by a reduced number of nodes. This is reflected in a reduced computation time when solving a limited set of ODEs.

A comparison of the computation time afforded by the 1D model with that required for the 2D model in ref. [26] was carried out. For the 1D model, all simulations were conducted with the academic version of MATLAB R2021a using an Intel (R) Core(TM) i7-10,610U CPU @ 180 GHz. According to ref. [26], the charging and discharging simulations for the 2D model, with results shown in Figure 18, required a maximum computation time of 0.7 s (with an average time of 0.25 s). This computation time was quantified using an Intel(R) Core(TM) i7-4600U CPU @ 2.10 GHz. However, achieving such an effective performance when solving the extensive set of 450 ODEs representing the 2D model required the adoption of the SundialsTB MATLAB toolbox (not available in MATLAB R2021a as it was developed by a third party), the sparse reverse Cuthill–McKee ordering algorithm to generate a banded Jacobian with a bandwidth of 9 and the CVODE solver with a banded Jacobian option.

For a fair comparison with the 1D model presented in this paper, the built-in *ode15s* function (with a banded Jacobian option) for solving stiff ODEs available in MATLAB R2021a
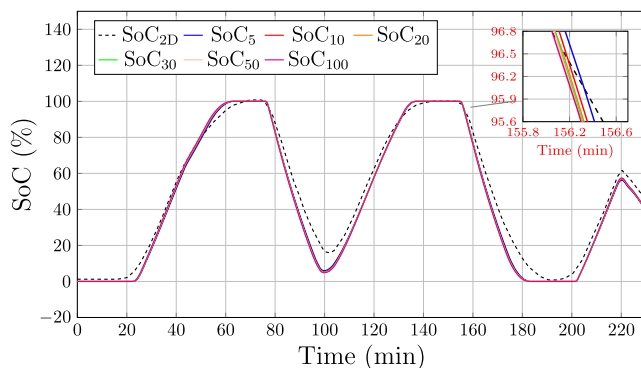
was adopted. This required defining a Jacobian with a bandwidth of 4. The average computation times for charging, discharging and cyclic charging–discharging processes afforded by the 1D models with different number of nodes are presented in Table 7. The simulation for charging processes required approximately half the average time reported in ref. [26] (i.e. 0.25 s) for most 1D models. For both the discharging and cyclic charging–discharging processes, the 1D models exhibited computation times comparable to that of the 2D model, averaging 0.28 s for discharging and not exceeding 0.65 s for cyclic processes. These computation times afforded by the 1D models are competitive despite not requiring the adoption of advanced solvers.

Notably, the 1D model employing only five nodes exhibits a high accuracy that is comparable to a model with 100 nodes (see Table 5), while demanding only 0.09 s for the charging process (less than half the average time of the 2D model), 0.12 s for discharging (roughly half the average time of the 2D model) and 0.34 s for the cyclic charging–discharging process (about half the maximum time registered by the 2D model).

5.3 | On the verification of the 1D model with 3D simulations

Although the presented 1D model has proven to be effective in accurately calculating key variables to assess heat transfer of the LHTES unit (i.e. the output temperature of the HTF and SoC of the thermal store), it would be desirable to undertake a comprehensive verification of the internal temperatures obtained with the model. This is because these variables are not easily accessible in experimental platforms as LHTES units may not incorporate internal sensors.

To this end, it would be suitable to conduct computational fluid dynamics (CFD) simulations of the thermal store under investigation. However, this is a non-trivial exercise requiring the development and verification of a complex 3D model—which would represent a standalone piece of work. Given that this paper is centred on the development of a 1D model, conducting simulations using CFD tools for further validation of the proposed model falls out of the scope of this paper.

FIGURE 20 Comparison of the SoC calculated with the 2D model from [26] and 1D models with different number of nodes using the method in Appendix B.

TABLE 7 Summary of the computation times of 1D models for charging, discharging and cyclic charging–discharging process with different number of nodes.

	Computation time (s)		
Nodes	**Charging**	**Discharging**	**Charging–discharging**
5	0.09	0.12	0.34
10	0.1	0.15	0.38
20	0.1	0.21	0.42
30	0.12	0.28	0.44
40	0.12	0.36	0.48
50	0.15	0.6	0.65

6 | CONCLUSIONS

A simplified 1D low-order dynamic model of an LHTES unit for heating applications based on a shell and tube internal configuration was presented in this paper. The model, despite its simplicity, considers a detailed mathematical description of the heat transfer between the components of the thermal store. The thermophysical properties of the PCM and HTF are accurately characterised in the model using polynomial functions which consider their temperature dependence. In particular, the specific heat curve as a function of temperature is represented with PDFs to describe the PCM's phase transition. Such an approach enables modelling different types of PCM, including those with an enthalpy hysteresis, by modifying the dimensionless parameters of the PDFs. This may be particularly useful when the specific heat curves for the storage medium of a practical storage unit are not available. The model can be also easily adapted to different internal geometries of the thermal stores and extended to cooling applications.

The modelling approach leads to a 1D representation of the LHTES unit which is significantly simpler than its 2D counterpart. For instance, a 1D model with 10 ODEs exhibits comparable results as those obtained with a 2D model represented by 450 ODEs despite the number of equations being reduced by 98%.

The model can be easily programmed in any software platform comprising an ODE solver. This is achieved by an implementation based on a set of nested ODEs and the use of look-up tables. Such a portability of the 1D model enables its inclusion into more complex thermal systems which also consider thermal sources, thermal loads, hydraulic components and thermal stores.

The 1D model was built in MATLAB/Simulink using S-functions and run with MATLAB's *ode15s* solver to demonstrate the versatility of its implementation. To verify its effectiveness and accuracy, simulation results afforded with the 1D model were compared against experimental data and the simulation results of a 2D model available in the literature. The results show that the effectiveness of the 1D model in calculating the output temperature of the HTF is not affected despite its simplicity. This is evidenced by the small values of error when the simulation results are compared against the experimental data. For instance, a 1D model represented by 10 ODEs exhibits an RMSE of ≤0.53 °C and an MAE of ≤0.32 °C when compared with the experimental measurements of the HTF's output temperature for charging and discharging operations.

Notably, the 1D model with five nodes yields a satisfactory RMSE of 0.47 kWh and an MAE of 0.39 kWh when the total stored energy is compared to that obtained with a 2D model. An improved computation efficiency while maintaining a comparable accuracy is exhibited by the 1D model without the need for advanced solvers. Executing a 1D model with five nodes for charging and discharging processes requires less than half the time (0.09 and 0.12 s) compared to that of a 2D model (0.25 s) requiring the CVODE solver from the SundialsTB toolbox.

CONFLICT OF INTEREST STATEMENT
The authors declare no conflicts of interest.

DATA AVAILABILITY STATEMENT
Data will be available on request.

ORCID
Hector Bastida [ID] https://orcid.org/0000-0001-8192-128X

REFERENCES

1. Xu, T., et al.: Latent heat storage integration into heat pump based heating systems for energy-efficient load shifting. Energy Convers. Manag. 236, 114042 (2021). https://doi.org/10.1016/j.enconman.2021.114042
2. Siddiqui, S., Macadam, J., Barrett, M.: The operation of district heating with heat pumps and thermal energy storage in a zero-emission scenario. Energy Rep. 7, 176–183 (2021). https://doi.org/10.1016/j.egyr.2021.08.157
3. Heier, J., Bales, C., Martin, V.: Combining thermal energy storage with buildings — a review. Renew. Sustain. Energy Rev. 42, 1305–1325 (2015). https://doi.org/10.1016/j.rser.2014.11.031
4. Reddy, K.S., Mudgal, V., Mallick, T.K.: Review of latent heat thermal energy storage for improved material stability and effective load management. J. Energy Storage. 15, 205–227 (2018). https://doi.org/10.1016/j.est.2017.11.005
5. Pintaldi, S., et al.: Energetic evaluation of thermal energy storage options for high efficiency solar cooling systems. Appl. Energy. 188, 160–177 (2017). https://doi.org/10.1016/j.apenergy.2016.11.123
6. Sarbu, I., Dorca, A.: Review on heat transfer analysis in thermal energy storage using latent heat storage systems and phase change materials. Int. J. Energy Res. 43(1), 29–64 (2019). https://doi.org/10.1002/er.4196
7. Frederiksen, S., Werner, S.: District Heating & Cooling. Studentlitteratur Ab, Lund (2013)
8. Dinçer, I., Rosen, M.A.: Thermal Energy Storage: Systems and Applications. John Wiley & Sons, West Sussex (2011)
9. Phase change materials | energy technologies. CRODA International Plc. https://www.crodaenergytechnologies.com/en-gb/functions/phase-change-materials Accessed 16 Sept 2022
10. Pointner, H., Steinmann, W.D.: Experimental demonstration of an active latent heat storage concept. Appl. Energy. 168, 661–671 (2016). https://doi.org/10.1016/j.apenergy.2016.01.113
11. Yağlı, H., et al.: Parametric optimization and exergetic analysis comparison of subcritical and supercritical organic Rankine cycle (ORC) for biogas fuelled combined heat and power (CHP) engine exhaust gas waste heat. Energy. 111, 923–932 (2016). https://doi.org/10.1016/j.energy.2016.05.119
12. Li, Z., et al.: Applications and technological challenges for heat recovery, storage and utilisation with latent thermal energy storage. Appl. Energy. 283, 116277 (2021). https://doi.org/10.1016/j.apenergy.2020.116277
13. Dancker, J., Wolter, M.: Improved quasi-steady-state power flow calculation for district heating systems: a coupled Newton-Raphson approach. Appl. Energy. 295, 116930 (2021). https://doi.org/10.1016/j.apenergy.2021.116930
14. Guo, F., Yang, X.: Long-term performance simulation and sensitivity analysis of a large-scale seasonal borehole thermal energy storage system

for industrial waste heat and solar energy. Energy Build. 236, 110768 (2021). https://doi.org/10.1016/j.enbuild.2021.110768

15. Huang, W., et al.: Multienergy networks analytics: standardized modeling, optimization, and low carbon analysis. Proc. IEEE. 108(9), 1411–1436 (2020). https://doi.org/10.1109/JPROC.2020.2993787

16. Zhong, Y., et al.: Day-ahead hierarchical steady state optimal operation for integrated energy system based on energy hub. Energies. 11(10), 2765 (2018). https://doi.org/10.3390/en11102765

17. Tafone, A., et al.: Innovative cryogenic phase change material (PCM) based cold thermal energy storage for liquid air energy storage (LAES) — numerical dynamic modelling and experimental study of a packed bed unit. Appl. Energy. 301, 117417 (2021). https://doi.org/10.1016/j.apenergy.2021.117417

18. Waser, R., et al.: Fast and experimentally validated model of a latent thermal energy storage device for system level simulations. Appl. Energy. 231, 116–126 (2018). https://doi.org/10.1016/j.apenergy.2018.09.061

19. Kurnia, J.C., Sasmito, A.P.: Numerical investigation of heat transfer performance of a rotating latent heat thermal energy storage. Appl. Energy. 227, 542–554 (2018). https://doi.org/10.1016/j.apenergy.2017.08.087

20. Vogel, J., Johnson, M.: Natural convection during melting in vertical finned tube latent thermal energy storage systems. Appl. Energy. 246, 38–52 (2019). https://doi.org/10.1016/j.apenergy.2019.04.011

21. Ezzat, Y., Abdel-Rehim, A.A.: Numerical modelling of lauric acid phase change material using iterative and non-iterative time-advancement schemes. J. Energy Storage. 53, 105173 (2022). https://doi.org/10.1016/j.est.2022.105173

22. Privitera, E., et al.: Impact of geometry on a thermal-energy storage finned tube during the discharging process. Energies. 15(21), 7950 (2022). https://doi.org/10.3390/en15217950

23. Zhang, C., Li, J., Chen, Y.: Improving the energy discharging performance of a latent heat storage (LHS) unit using fractal-tree-shaped fins. Appl. Energy. 259, 114102 (2020). https://doi.org/10.1016/j.apenergy.2019.114102

24. Gasia, J., et al.: Numerical study of dynamic melting enhancement in a latent heat thermal energy storage system. J. Energy Storage. 31, 101664 (2020). https://doi.org/10.1016/j.est.2020.101664

25. Gholamibozanjani, G., Farid, M.: Experimental and mathematical modeling of an air-PCM heat exchanger operating under static and dynamic loads. Energy Build. 202, 109354 (2019). https://doi.org/10.1016/j.enbuild.2019.109354

26. Barz, T., et al.: Experimental analysis and numerical modeling of a shell and tube heat storage unit with phase change materials. Ind. Eng. Chem. Res. 55(29), 8154–8164 (2016). https://doi.org/10.1021/acs.iecr.6b01080

27. Wan, H., et al.: Development of a quasi-2D variable resistance–capacitance model for tube-encapsulated phase change material storage tanks. Appl. Therm. Eng. 214, 118868 (2022). https://doi.org/10.1016/j.applthermaleng.2022.118868

28. Bastida, H., et al.: Dynamic modelling of ice-based thermal energy storage for cooling applications. IET Energy Syst. Integr. 4(3), 317–334 (2022). https://doi.org/10.1049/esi2.12061

29. De la Cruz-Loredo, I., Ugalde-Loo, C.E., Abeysekera, M.: Dynamic simulation and control of the heat supply system of a civic building with thermal energy storage units. IET Generat. Trans. Distribut. 16(14), 2864–2877 (2022). https://doi.org/10.1049/gtd2.12453

30. Mao, Q., et al.: A novel heat transfer model of a phase change material using in solar power plant. Appl. Therm. Eng. 129, 557–563 (2018). https://doi.org/10.1016/j.applthermaleng.2017.10.038

31. Home | INEOS Olefins & Polymers Europe. INEOS Group. https://www.ineos.com/businesses/ineos-olefins-polymers-europe/ Accessed 14 July 2022

32. Marlotherm, S.H.: Heat Transfer Fluid. Eastman Chemical Company. https://www.eastman.com/en/products/product-detail?product=71114174&pn=marlotherm+sh+heat+transfer+fluid Accessed 16 Sept 2022

33. Aisi 316 stainless steel. Material Properties Database. https://www.makeitfrom.com/compare/AISI-316-S31600-Stainless-Steel/EN-1.0345-P235GH-Non-Alloy-Steel Accessed 16 Sept 2022

34. Portable liquid ultrasonic flow meter | FLUXUS F601. Flexible Industriemesstchnig GmbH. http://www.flexim.com/en/product/fluxus-f601 Accessed 24 June 2022

35. Bastida, H., et al.: Dynamic modeling and control of a plate heat exchanger. In: 1st IEEE Conference on Energy Internet and Energy System Integration(EI2), pp. 1–6 (2017)

36. Bastida, H., et al.: Dynamic modelling and control of counter-flow heat exchangers for heating and cooling systems. In: 2019 54th International Universities Power Engineering Conference (UPEC), pp. 1–6 (2019)

37. Bastida, H., et al.: Modelling and control of district heating networks with reduced pump utilisation. IET Energy Syst. Integrat. 3(1), 13–25 (2021). https://doi.org/10.1049/esi2.12001

38. De la Cruz-Loredo, I., et al.: Experimental validation of a hybrid 1-D multi-node model of a hot water thermal energy storage tank. Appl. Energy. 332, 120556 (2023). https://doi.org/10.1016/j.apenergy.2022.120556

39. Diaconu, B.M., Varga, S., Oliveira, A.C.: Experimental assessment of heat storage properties and heat transfer characteristics of a phase change material slurry for air conditioning applications. Appl. Energy. 87(2), 620–628 (2010). https://doi.org/10.1016/j.apenergy.2009.05.002

40. Musavi, S.M., et al.: Thermal energy storage property and temperature control performance of phase change materials eutectic mixture nano-composite. Micro Nanosyst. 14(3), 272–280 (2022). https://doi.org/10.2174/1876402913666210903162938

41. Barz, T., et al.: State and state of charge estimation for a latent heat storage. Control Eng. Pract. 72, 151–166 (2018). https://doi.org/10.1016/j.conengprac.2017.11.006

42. Bastida, H., De la Cruz-Loredo, I., Ugalde-Loo, C.E.: Effective estimation of the state-of-charge of latent heat thermal energy storage for heating and cooling systems using non-linear state observers. Appl. Energy. 331, 120448 (2023). https://doi.org/10.1016/j.apenergy.2022.120448

APPENDIX A

LHTES UNIT PARAMETERS

The parameters of the shell and tube LHTES unit investigated in this paper, for a single tube, are provided in Table A1.

The thermophysical properties of the HTF (Marlotherm SH) are described by the following equations:

$$\rho_f = -0.71482T + 1058.4, \tag{A1}$$

$$c_{p,f} = 3.7263T + 1474.5, \tag{A2}$$

$$k_f = -0.00013184T + 0.13326, \tag{A3}$$

$$\mu_f = 10113T^{-1.755}, \tag{A4}$$

where T is used to indicate temperature (°C), and ρ_f (kg/m³), $c_{p,f}$ (J/(kg°C)), k_f (W/(m°C)), and u_f (Ns/m²) are the density, specific heat, thermal conductivity and dynamic viscosity of the HTF.

TABLE A1 Parameters of shell and tube TES unit (single tube) [26].

Parameter	Symbol	Value	Unit
Tube external radius	r_o	8.25	mm
Tube internal radius	r_i	6.75	mm
Tube hydraulic diameter	D_t	13.5	mm
Tube length	L	2.5	m
Heat transfer area	A_{tr}	0.1060	m^2
Cross sectional area	A_c	1.4314×10^{-4}	m^2
HTF volume	V_f	3.5785×10^{-4}	m^3
Thermal conductivity of the tube (P235GH)	k_t	50	W/(m°C)
Radius of PCM	r_p	19.9774	mm
Cross sectional area of PCM	A_p	0.00104	m^2
PCM volume	V_p	0.0026	m^3

The density ρ_p (kg/m^3) and the thermal conductivity k_p (W/(m°C)) of the PCM (RigidexHD6070EA) are given by the following equations:

$$\rho_p = \frac{167.2182}{1.0 + e^{[0.078916(T-129.9861)]}} + 760.8218, \quad \text{(A5)}$$

$$k_p = \frac{0.41857}{1.0 + e^{[0.036647(T-96.162)]}} + 0.15406. \quad \text{(A6)}$$

APPENDIX B

SoC CALCULATION METHOD

SoC quantification is directly related to the storage capacity of the LHTES unit, determined by the specific latent heat Δh_{φ^G} of the PCM. The total value of Δh_{φ^G} for the thermal store under study is 259.61 kJ/kg [42]. The phase transition zone, where Δh_{φ^G} is absorbed or released during the solid–liquid transformation, may be limited within the specific heat–temperature curve through the temperatures $T_{empty} = 109.5$ °C and $T_{full} = 138$ °C (see Figure B1). Thus, if the PCM temperature is below T_{empty}, Δh_{φ^G} has been fully released, indicating a complete discharge so that SoC is 0%. In contrast, when the PCM temperature exceeds T_{full}, Δh_{φ^G} has been absorbed, denoting full charging and SoC is 100%. This relationship is described mathematically as the following equation:
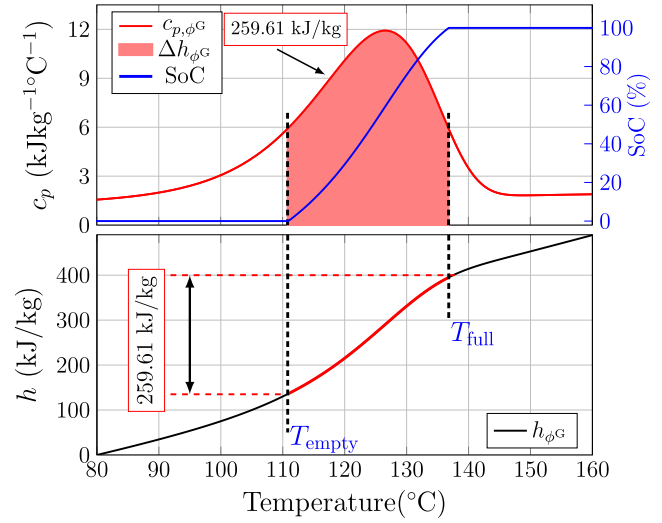
FIGURE B1 PCM's specific heat–temperature curve using a Gumbel PDF and SoC calculation using (B1). The pink shaded area limited by T_{full} and T_{empty} is Δh_{φ^G}. (b) Specific enthalpy [42].
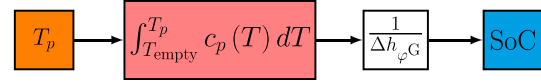
FIGURE B2 Schematic of the method to calculate SoC [42].

$$\text{SoC}_T(T) = \begin{cases} 100 & T_p > T_{full} \\ \dfrac{\int_{T_{empty}}^{T_p} c_p(T)dT}{\Delta h_{\varphi^G}} & T_{empty} \leq T_p \leq T_{full}, \\ 0 & T_p < T_{empty} \end{cases} \quad \text{(B1)}$$

Equation (B1) is used for all node temperatures in the model, with N denoting the number of nodes. Thus, the SoC for the whole PCM volume within the LHTES unit is defined by the following equation:

$$\text{SoC} = \frac{\sum_{i=1}^{N} \text{SoC}_{T_i}}{N} \quad \text{(B2)}$$

Figure B2 shows a high-level schematic diagram to illustrate the SoC calculation method, where the integration of the specific heat–temperature curve is carried out within the defined temperature limits and T_p is the PCM temperature. For a more comprehensive understanding of the method, interested readers may refer to ref. [42].